International Journal of Mechanical, Industrial and Aerospace Sciences
ISSN: 2517-9950
Vol:10, No:5, 2016

Characterization of the Near-Wake of an Ahmed Body Profile

Stéphanie Pellerin, Bérengère Podvin, Luc Pastur

Abstract—In aerovehicles context, the flow around an Ahmed body profile is simulated using the velocity-vorticity formulation of the Navier-Stokes equations, associated to a penalization method for solids and Large Eddy Simulation for turbulence. The study focuses both on the ground influence on the flow and on the dissymetry of the wake, observed for a ground clearance greater than 10% of the body height H. Unsteady and mean flows are presented and analyzed. POD study completes the analysis and gives information on the most energetic structures of the flow.

Keywords—Ahmed body, bi-stability, LES, near wake.

I. Introduction

DRAG reduction of separated flows are current topics of automobile industry applications. A thorough understanding of the physics of unsteady separation in the absence of control is therefore required in order to define and evaluate the action of upstream wall actuators. More than 30% of the drag of automobile vehicles is due to phenomena that occur in the vicinity of the rear window, which emphasizes the necessity to modify the vortex dynamics in the recirculation region and in the near wake.

II. Numerical Approach

A. Large Eddy Simulation Using the $(v-\omega)$ Formulation

The numerical method is based on the $(v-\omega)$ velocity-vorticity formulation for incompressible flows, allowing an accurate simulation of a given configuration and a direct manipulation of the flow through modification of the vorticity at the boundary. The turbulent behavior is modeled with Large Eddy Simulation using the filtered Navier-Stokes equations obtained by means of the subgrid decomposition. The exact field is split into filtered variables and subgrid variables. The filtered Navier-Stokes equations using the $(v-\omega)$ formulation are given as:

$$\frac{\partial \omega}{\partial t} - \nabla \times (v \times \omega) = -Re^{-1}\ \nabla \times \nabla \times \omega + \nabla \times \tau \quad (1)$$

$$\omega = \nabla \times v \qquad \nabla \cdot v = 0 \quad (2)$$

where Re is the Reynolds number, v the filtered velocity vector and ω its curl, resolved on the grid. The vector τ representing the subgrid scale contributions is function of the subgrid viscosity ν_{sgs}, as follows, $\tau = -\frac{\nu_{sg}}{Re}\ \nabla \times \omega$. The mixed scale subgrid model, developed in LIMSI [1], is chosen is this study:

$$\nu_{sg} = \left(C_S^2 \Delta^2 \|\omega\|\right)^{\alpha} \left(C_B \Delta \|\mathbf{u}'\|\right)^{(1-\alpha)} \quad (3)$$

where k corresponds to a kinetic energy associated with the subgrid cell. Classical vorticity and TKE models are respectively obtained for values 0 or 1 of the exponent α, taken equal to 0.5 in this study. C_S and C_B correspond respectively to the Smagorinsky and Bardina constants. Δ is a characteristic length of the local cell. This model has the advantage to damp smoothly the eddy viscosity in the regions where all the scales are well resolved.

B. Penalization Method

Solid are modelled through a penalization method, adapted to the $(v-\omega)$ formulation of the Navier-Stokes equations. The velocity and vorticity fields are imposed equal to zero inside the solids. The vorticity vector needs to be zero inside the solid at each time step, which is enforced by setting $\frac{\partial \omega}{dt} = 0$. The diffusive terms of (1) are cancelled, at each time step, using a penalization matrix. On a given solid surface, the tangential velocity is zero. The vorticity field at the wall (tangential components) is then calculated from velocity derivatives.

C. Resolution

A M.A.C. staggered grid is used for the spatial discretization. Time and spatial discretizations use 2nd order schemes. The coupled Helmholtz problem of the vorticity transport equation is solved with a block Jacobi iterative algorithm. The velocity field is then obtained through a projection method [2].

An infinite upstream velocity U_∞ is imposed at the inlet of the domain from which the tangential components of the vorticity are deduced. Perturbations (white noise) are superimposed on them to obtain the correct development of the turbulent flow. At the outlet surface, a convective transport hypothesis is applied (viscous effects $(v-\omega)$ neglegted). The vorticity tangential components are calculated using an extrapolation along the characteristics. In the vertical direction y, slip conditions are imposed at the lower and upper surfaces. A periodicity condition is used for the transverse direction z.

III. Modelization

The chosen configuration is an Ahmed body [3] which has a sharp rear corner, above a flat surface. It models a ground vehicle on the road. The characteristic length of the problem

Stéphanie Pellerin is with the LIMSI-CNRS, Univ. Paris-Sud, Université Paris Saclay, Bât 508, Rue John Von Neumann, 91403 Orsay Cedex, France (e-mail: pellerin@limsi.fr).
Bérengère Podvin is with the LIMSI-CNRS, Université Paris-Saclay, Bât 508, Rue John Von Neumann, 91403 Orsay Cedex, France.
Luc Pastur is with the LIMSI-CNRS, Univ. Paris-Sud, Université Paris Saclay, Bât 508, Rue John Von Neumann, 91403 Orsay Cedex, France.

is the body height H. A set of geometries have been tested, using as reference the experimental model of Grandemange *et al.* [4]. The Ahmed body has a bluff shape in both transverse directions. Most of the simulations performed used a body with a lenght L about 3.63 H and a spanwise dimension l about 1.35 H [3]. Much effort has been put into making the numerical configuration similar to the experiment [4].

For this 3D unsteady turbulent flow, the grids used depend on the domain size considered and vary from about 5 to 10 million points. The flow develops along the streamwise direction x, on a regular grid. The spanwise mesh in the direction z is also associated with a regular discretization. Only the vertical direction y is inhomogeneous. The mesh is refined at the top and the bottom of the body. In most of the cases presented here, the Ahmed body is modelled using $nx_A(228) \times ny_A(65) \times nz_A(49)$ points.

The computational domain corresponds to L_x from 8 to 11 H, L_y to 1.8 H and L_z from 2 to 3 H. The Ahmed body is centered in the computational domain along the z direction. The wake can develop over $1.1 - 1.9$ L after the end of the body and the last separation on the roof.

IV. Results

Simulation of an incompressible 3D turbulent flow around an Ahmed body is then performed using LES, the $(v - \omega)$ formulation and an adapted penalization method for the Ahmed body and the flat plate if its occurs. Experiments have shown that the flow is characterized by a bi-stability behavior, between two conjugated reflectional symmetry-breaking (RSB) wakes [5]. The existence and the mode switching dynamics, which depend on the ground clearance of the Ahmed body C, constitutes the focus of our study. A non-dimensional ground clearance is then defined $C^* = C/H$.

Simulations are performed for $Re = 1.7 \times 10^4$, based on U_∞ = 10 m $\cdot$ s^{-1}, the fluid viscosity ν_{air} and the body height H. The flow is initially at rest. The flow develops over a rather long time to obtain a turbulent unsteady state [8]. For different cases with and without ground, the unsteady flow is studied through velocity and vorticity fields, and the mean flow is analyzed, focusing on dissymmetry of the near wake. The turbulent statistics of the flow are computed. The pressure field is of particular interest as it is a quantity readily accessible in experiments.

A. Unsteady Field

The unsteady fields in Figs. 1 to 4 show a 3D fully turbulent flow, with a large set of scales and numerous vortices, convected with the wake. The spanwise component of the vorticity ω_z is represented in Fig. 1, in a middle vertical plane (xy). Two separation zones occur close to the front of the body and at the end of the body numerous vortices are ejected in the mixing zone. When the ground clearance C decreases, the shedding progressively disappears at the bottom of the body, and the wake is progressively attracted by the ground.

Fig. 2 represents the vertical component of the vorticity ω_y in horizontal planes (zx) (top-view), without ground. The two separation zones at each side are rather symmetric and the alternated shedding vortices are convected in the wake. The wake is only influenced by the shape of the body. At the top of the Ahmed body, the flow is less disturbed.

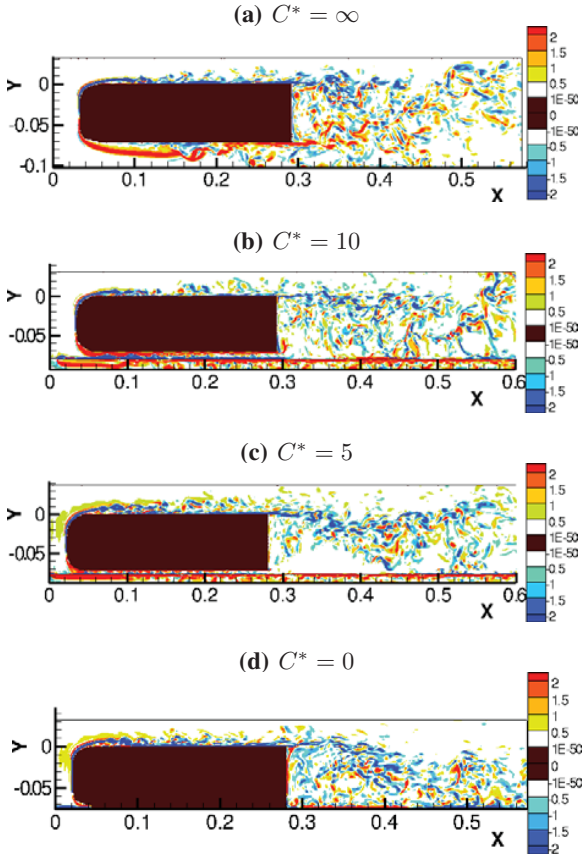

Fig. 1 Unsteady field: Spanwise vorticity ω_z in a middle plane (xy), (a) $C* = \infty$ (without ground), (b) with a ground for $C* = 10$, (c) for $C* = 5$ and (d) for $C* = 0$ (body on the ground)

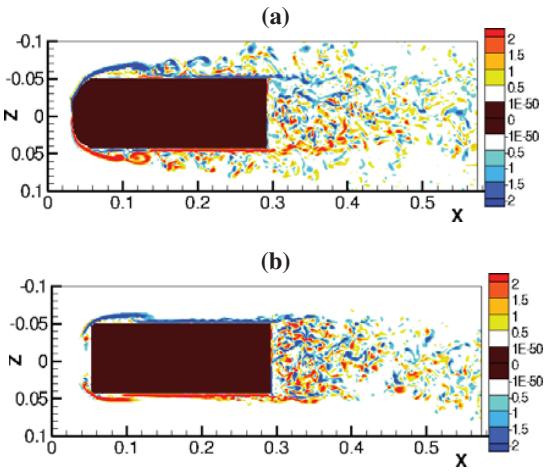

Fig. 2 Unsteady field without ground, $C^* = \infty$: Vertical vorticity ω_y in top-view horizontal planes (zx), at (a) half-height of the body and (b) $1/100$ H from the top of the body

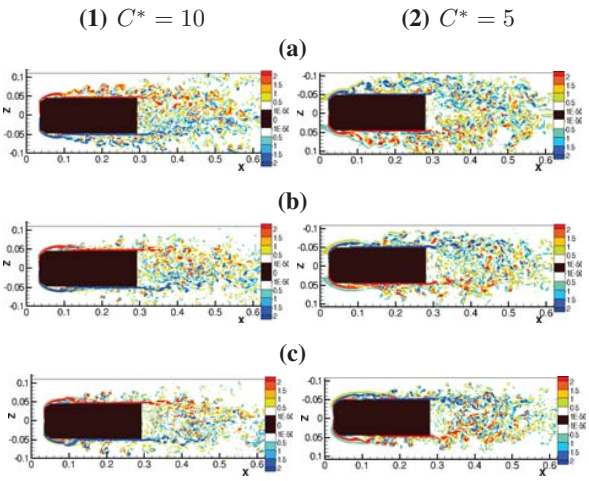

Fig. 3 Unsteady field in presence of a flat plate (ground): Vertical vorticity ω_y in top-view horizontal planes (zx), for two ground clearances C^*, at different distances from the top of the body, (a) $3/4\ H$, (b) $1/2\ H$, (c) $1/4\ H$

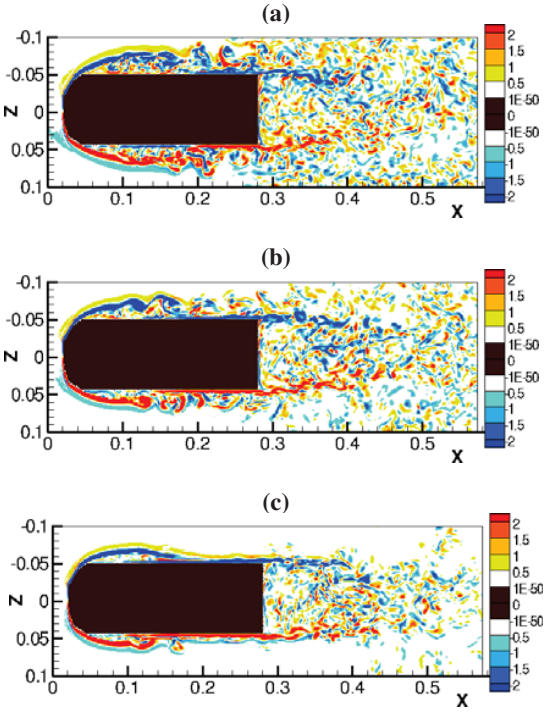

Fig. 4 Unsteady field when the body is on the ground, $C^* = 0$: Vertical vorticity ω_y in top-view horizontal planes (zx), at different distances from the top of the body, (a) $3/4\ H$, (b) $1/2\ H$, (c) $1/4\ H$

For the cases with a ground (Figs. 3 and 4), clear differences are observed between the bottom and the top of the body, due to the presence of the wall. The ground modifies clearly the wake over half of the body height for $C^* = 10$ (Fig. 3). In contrast, its effects are felt over the full body height, in the case of a body on the ground for $C^* = 0$ (Fig. 4).

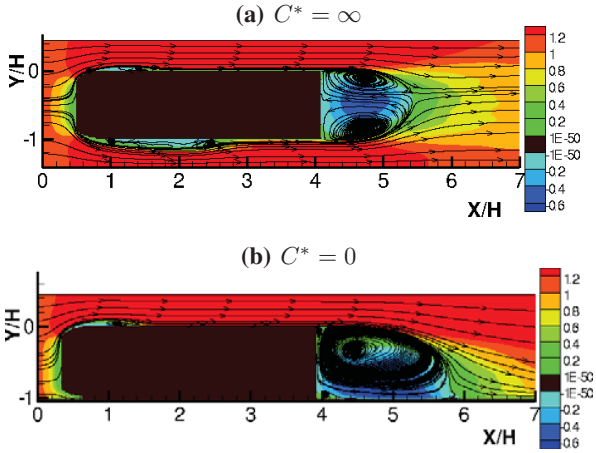

Fig. 5 Mean field: Longitudinal velocity $< v_x >$ and stream function in a middle plane (xy), (a) without ground $C^* = \infty$ and (b) $C^* = 0$

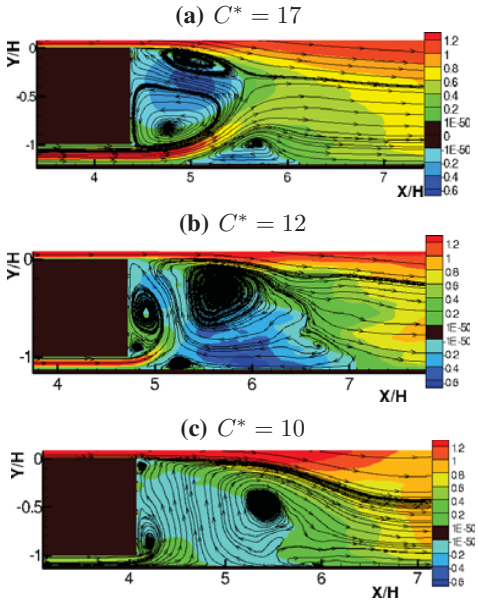

Fig. 6 Zooms of mean field in the vicinity of the back face: Longitudinal velocity $< v_x >$ and stream function in a middle plane (xy), in presence of a flat plate

B. Mean Field

The mean flow is calculated using a set of unsteady fields recorded successively, over a time-integration interval which may depends on the case considered. Fig. 5 represents the time-averaged streamlines of the flow, projected in the vertical mid-plane (xy), colored by the time-averaged longitudinal velocity $< v_x >$. A first recirculation zone is well described on the roof. The second equivalent zone, on the bottom of the body, interacts progressively with the boundary layer and then disappears when the clearance C decreases. In case without ground (Fig. 5 (a)), the two recirculation zones in the wake are rather symmetric and their lengths can be estimated approximately about $1.2H$.

Fig. 6 zooms in the near-wake for different values of C^*. When C^* increases from 0, the behavior of the downstream

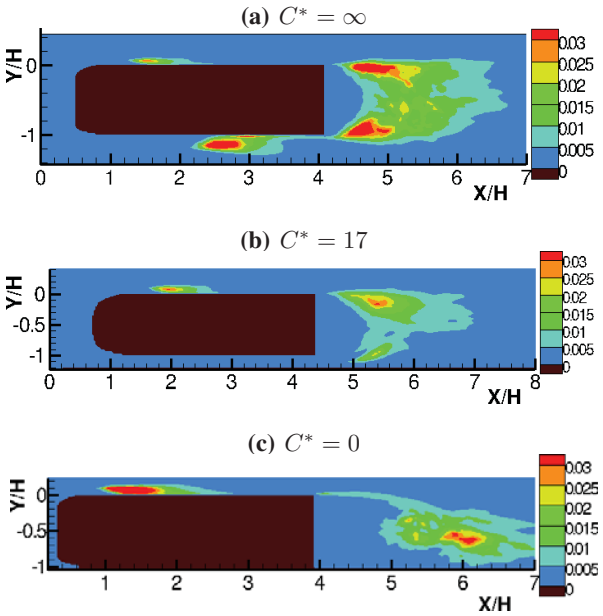

Fig. 7 Mean field: Turbulent kinetic energy k and stream function in a middle plane (xy), (a) without ground $C^* = \infty$, (b) with a ground for $C^* = 17$ and (c) on the ground $C^* = 0$

recirculation zones changes considerably. The velocity of the flow increases under the body and the lower recirculation zone appears and grows. The length of the zones also increases until about $2.5H$.

The turbulent kinetic energy $k = \frac{1}{2}\sum < v_i'^2 >$ is represented in Fig. 7, where v_i' is the time fluctuation of the velocity component v_i. The maxima values are rather symmetric in the case without ground. The lower maximum disappears progressively when C decreases.

Fig. 8 represents the time-averaged streamlines of the flow, projected in a horizontal mid-plane (zx) or top-view, colored by the time-averaged longitudinal velocity $< v_x >$. The influence of the ground clearance is evidenced. For $C^* = 0$, the wake is symmetric with respect to the (xy) mid-plane, whereas for $C^* > 0.1$ the left/right symmetry has been broken. This is in agreement with the so-called RSB-wakes observed experimentally, as shown for instance in [4], [5], beyond a critical value of C^*. The case $C^* = 0.1$ is not exactly symmetric due to slightly lack of convergence in the mean field. Note that the bistability phenomenon reported in [4], [5] has not been observed in our LES yet because the observation time is smaller than the mean value of the persistence time of the RSB wake. It is however expected that longer runs might exhibit transitions between both reflectional-conjugated wakes.

C. Proper Orthogonal Decomposition

POD (Proper Orthogonal Decomposition) is a statistical technique introduced by Lumley [6] in turbulence which extracts the spatial patterns (POD modes) which are best correlated with a spatio-temporal field on average. To solve the problem when the field spatial dimension is very large, Sirovich [7] introduced the method of snapshots, which makes

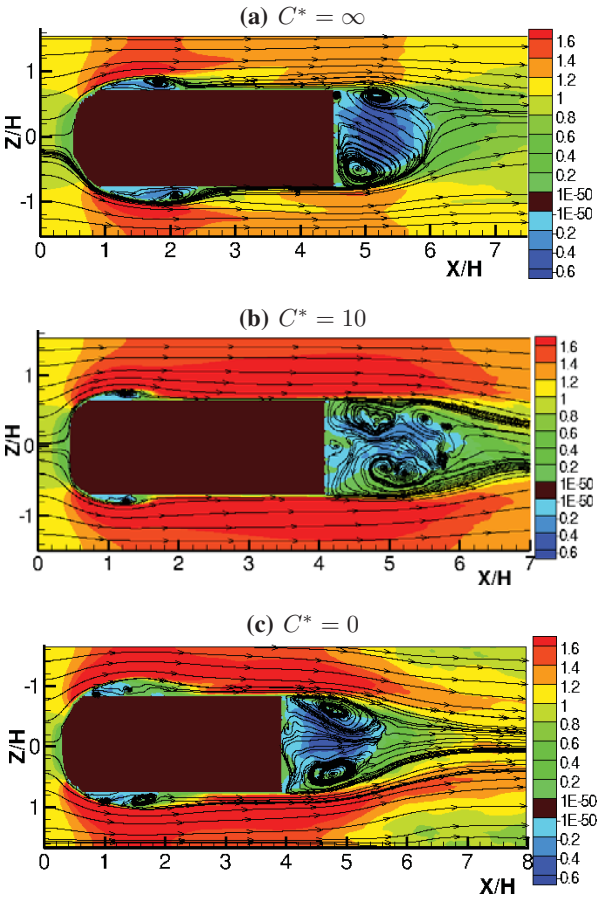

Fig. 8 Mean field: Longitudinal velocity $< v_x >$ and stream function in an half-body horizontal plane (zx), (a) without ground $C^* = \infty$, (b) with a ground for $C^* = 10$ and (c) on the ground $C^* = 0$

it possible to recover the POD spatial modes from the temporal autocorrelation tensor (instead of the spatial autocorrelation tensor in the original method proposed by Lumley).

POD was applied to the 3D velocity fields over the full domain for the two limiting cases of $C^* = \infty$ (no ground effect) and $C^* = 0$ (body on the ground). The idea is to write the velocity field as:

$$\underline{u}(x, y, z, t) = \sum_n a^n(t)\underline{\phi}^n(x, y, z) \tag{4}$$

where $\underline{\phi}^n(x, y, z)$ represents the spatial pattern or POD mode and $a^n(t)$ represents the temporal amplitude of the mode. By construction the POD modes are orthogonal and the temporal amplitudes are uncorrelated i.e.:

$$< a^n(t)a^m(t) >= \delta_{nm}\lambda^n \tag{5}$$

where $<>$ represents a time average, δ_{mn} is the Krönecker symbol and λ^n is the energy of the POD mode n.

The first POD mode corresponds to the mean mode of velocity described in the Section IV-B, as can be seen in Fig. 9 for an horizontal mid-plane. The mean pressure on the same plane is also shown in Fig. 10 for both limiting cases $C^* = \infty$ and $C^* = 0$. This confirms that spanwise asymmetry is present

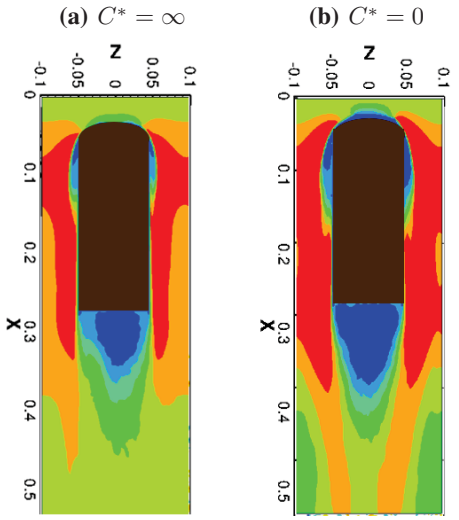

Fig. 9 Longitudinal velocity component v_x of the first POD mode on a horizontal plane (zx) at mid-height of the body, (a) without ground $C^* = \infty$ and (b) body on the ground $C^* = 0$

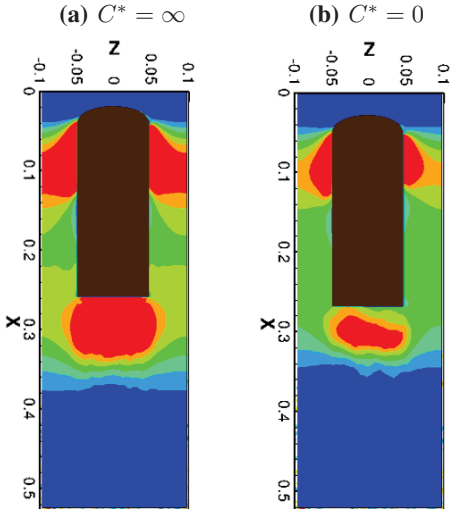

Fig. 10 First POD mode of the pressure field on a horizontal plane (zx) at mid-height of the body, (a) without ground $C^* = \infty$ and (b) body on the ground $C^* = 0$

when the distance between the body and the ground is large enough, but disappears when the body lies on the ground.

The POD spectrum representing the energy of the modes λ^n is presented in Fig. 11 and is seen to be quite similar for both cases. The next two most energetic modes are of nearly equal value and correspond to Von Karman-like modes, which represent the shedding of vortices behind the body. The two modes correspond to the travelling wave nature of the spatial pattern. This pattern in a longitudinal plane is represented in Fig. 12. The Von Karman-like street is clearly noticeable. The size of the vortices is about H.

The temporal amplitudes corresponding to these two modes are represented in Fig. 13. The wave-like nature of the mode is confirmed. The nondimensional characteristic frequencies

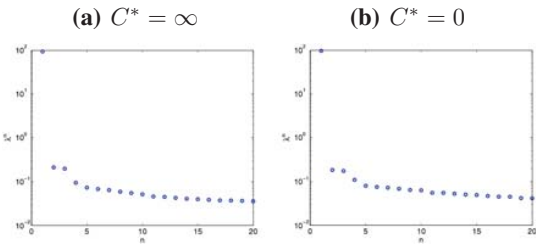

Fig. 11 POD spectrum of the full 3D velocity field, (a) without ground $C^* = \infty$ and (b) body on the ground $C^* = 0$

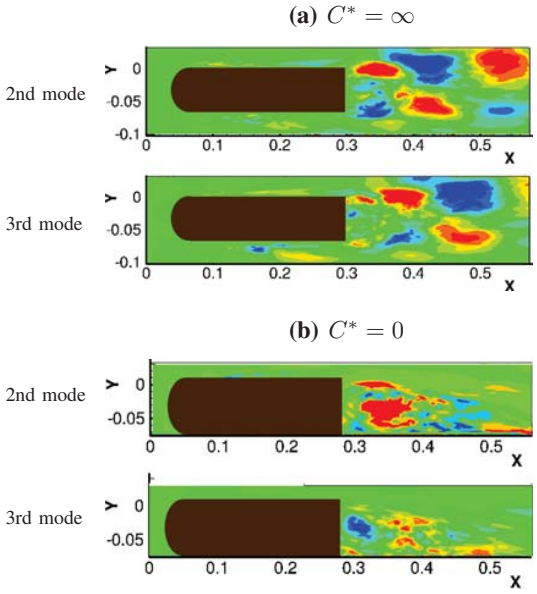

Fig. 12 Longitudinal velocity component v_x of the second and third POD modes in the mid-section longitudinal plane (xy), (a) without ground $C^* = \infty$ and (b) body on the ground $C^* = 0$

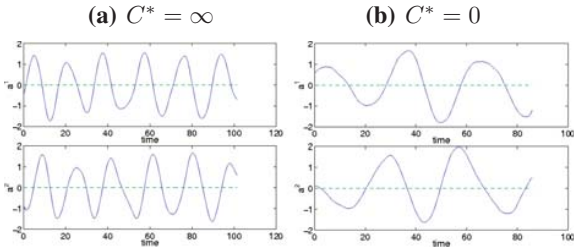

Fig. 13 Temporal amplitudes of the second and third POD modes for the longitudinal velocity v_x, as function of non-dimensional time. (a) without ground $C^* = \infty$ and (b) body on the ground $C^* = 0$

of the case $C^* = 0$ and $C^* = \infty$ are respectively $f_0 = 0.22$ and $f_\infty = 0.26$, in agreement with experimental observations [4].

V. Conclusion

The flow around an Ahmed body profile has been calculated using LES, the $(v - \omega)$ formulation and a penalization method for solids. The influence of the ground clearance on the symmetry of the wake has been evidenced. The

symmetry-breaking of the wake has been recovered by LES for large enough ground clearance. Switching dynamics was not observed due to simulation timing. This study allows us to extract from the full simulation of the flow the relevant spatial and temporal scales.

Acknowledgment

The authors would like to acknowledge Olivier Cadot and Antoine Evrard for fruitful discussions. This work has been supported by the LaSIPS contract TurbFork.

References

[1] L. Ta Phuoc, "Modèles de sous maille appliqués aux écoulements instationnaires décollés", *Proceedings of a DRET conference: Aérodynamique instationnaire turbulente - Aspects numériques et expérimentaux*, Paris, France: DGA/DRET editors, 1994.

[2] C. Tenaud, S. Pellerin, A. Dulieu and L. Ta Phuoc, "Large Eddy Simulations of a spatially developing incompressible 3D mixing layer using the $v\omega$ formulation", *Comput. Fluids*, vol. 34, pp. 67-96, 2005.

[3] S. R. Ahmed, G. Ramm and G. Faltin, "Some Salient Features of the Time-Averaged Ground Vehicle Wake", *SAE technical paper series*, No. 840300, Detroit, 1984.

[4] M. Grandemange, M. Gohlke and O. Cadot, "Turbulent wake past a three-dimensional blunt body. Part 1. Global modes and bi-stability", *J. Fluid Mech.*, vol. 722, pp. 51-84, 2013.

[5] O. Cadot, A. Evrard and L. Pastur, "Imperfect supercritical bifurcation in a three-dimensional turbulent wake", *Phys. Rev. E*, vol. 91, no. 6, 063005, 2015.

[6] P. Holmes, J. L. Lumley and G. Berkooz, *Turbulence, Coherent Structures, Dynamical Systems and Symmetry*, Cambridge University Press, 1996.

[7] L. Sirovich, "Turbulence and the dynamics of coherent structures part II: symmetries and transformations", *Q. Appl. Math.*, vol. 45, no. 3, 561–571, 1987.

[8] S. Pellerin and B. Podvin, "A study of the groung influence on the wake of an Ahmed body profile", *50th 3AF International Conference on Applied Aerodynamics*, Toulouse, France, 30-31 March, 1 April, 2015.